 DOI 10.1515/tjj-2012-0028 — Int. J. Turbo Jet-Engines 2012; 29(3): 207–215

C. R. Arun, Vasudevan Raghavan*

Numerical Parametric Studies of Laminar Flame Structures in Opposed Jets of Partially Premixed Methane-Air Streams

Abstract: Interactions of fuel-rich and fuel-lean mixtures and formation of interlinked multiple flame zones are observed in gas turbines and industrial furnaces. For fundamentally understanding such flames, numerical investigation of heat and mass transport, and chemical reaction processes, in laminar, counter flowing partially premixed rich and lean streams of methane and air mixtures, is presented. An axisymmetric numerical reactive flow model, with C2 detailed mechanism for describing methane oxidation in air and an optically thin radiation sub-model, is used in simulations. The numerical results are validated against the experimental results from literature. The equivalence ratios of counter flowing rich and lean reactant streams and the resulting strain rates have been varied. The effect of these parameters on the flame structure is presented. For a given rich and lean side equivalence ratios, by varying the strain rates, triple, double and single flame zones are obtained.

Keywords: partially premixed flames, double and triple flame structures, equivalence ratio, strain rate, optically thin radiation model, detailed kinetics mechanism

C. R. Arun: Department of Mechanical Engineering, Indian Institute of Technology Madras, Chennai, India 600036
***Corresponding author: Vasudevan Raghavan:** Department of Mechanical Engineering, Indian Institute of Technology Madras, Chennai, India 600036, E-mail: raghavan@iitm.ac.in

1 Introduction

Partially premixed flames are observed in several practical combustors. When compared to a pure diffusion flame or a premixed flame from stoichiometric air-fuel mixture, a partially premixed flame has more stability, lesser emission production and more controllability. Therefore, it is one of the main focuses of combustion research. Interactions of partially premixed streams and their flames occur in practical systems such as gas turbine combustors and industrial gas fuel fired furnaces, when the fuel-air mixing is not uniform. A few other examples of partial premixing are lifted flames in burners, domestic appliances and opposed fire spread over condensed fuel surfaces. In general, partially premixed flames are formed when the fuel stream of a diffusion flame is premixed with not enough quantity of oxidizer and/or the oxidizer stream is mixed with small amounts of fuel prior to the reaction zone. As a result, such flames can exhibit the characteristics of both premixed and diffusion flames. A pure premixed (stoichiometric fuel-air mixture) or a pure diffusion flame exhibits a single reaction zone. In partially premixed flames formed by the interaction of two streams having rich and lean equivalence ratios, multiple reaction zones, such as double flames or triple flames, may be formed. A double flame contains two reaction zones, identified as a rich premixed flame zone near to the fuel rich premixed stream and a lean flame zone near to the oxidizer rich premixed stream. A triple flame contains three reaction zones; one fuel-rich and other oxidizer-rich, as observed in double flames, and the third one, nearly non-premixed, located in-between them. These reaction zones are spatially separated, however, are synergistically coupled through thermochemical and fluid dynamic interactions between them. Each reaction zone is influenced by the other reaction zones, and the global flame structure is strongly dependent upon the factors like the equivalence ratios of the streams, their orientation such as co-flow or opposed-flow, and most importantly the strain rate.

Partially premixed flames have been studied both experimentally and numerically by several researchers. Hamins et al. (1985) investigated the double flame structures in a partially premixed flame stabilized between counter-flowing streams of heptane and methane, premixed with oxygen and nitrogen. They analyzed the two reaction zones and showed that for the flame to extinguish the reaction zones must merge. Seshadri et al. (1985) using large activation energy asymptotic with one-step chemistry showed that level of premixing increases the sensitivity of a flame to stretch-induced extinction. Rogg at al. (1986) compared the computed temperature and concentration profiles with experimental data available in the literature, thereby demonstrating the influence of

partial premixing in diffusion flames on the structure of turbulent non-premixed flames. Yamaoka et al. (1986) studied the double flame structure that occurred in partially premixed flames, using a porous cylinder burner. They analyzed the distance between the reaction zones as a function of equivalence ratio of the opposing streams. Smooke et al. (1988) performed experimental and numerical study of counter-flow, partially premixed, methane-air flames. The structure and extinction characteristics were reported in detail. Nishioka et al. (1994) studied the nitric oxide emission characteristics of counter-flow methane-air Bunsen burner flames with a double flame structure. They reported that the double flame produces more or less NO, depending on the equivalence ratio of rich mixture and on velocity gradients of the opposing streams. Tanoff et al. (1996) using detailed numerical calculations and experimental results investigated the sensitivity of the flame structures to fuel premixing and strain rate. They studied the changes produced in the structure and the corresponding effect on the degree of NO formation. Blevins and Gore (1998) reported a numerical study of low strain rate, partially premixed methane-air counter-flow flames. They investigated the variation produced in the flame structure with respect to the fuel side equivalence ratio. The effect of fuel side equivalence ratio on the NO formation and destruction in a low strain rate partially premixed flames was also reported. Ravikrishna and Laurendeau (2000) measured the NO concentration along the centerline of methane-air, counter-flow partially premixed flames, under atmospheric conditions, using the laser-induced fluorescence technique and verified it numerically using an opposed-flow flame code. Xue et al. (2002) studied the ability of reaction mechanisms to predict the structure of partially premixed counter-flow methane-air flames. The predicting capability of GRI-3.0 and C2 mechanism was verified against experimental measurements. They expressed the need of more extensive experimental data to validate mechanisms for partially premixed flames. Guo et al. (2006) carried out a numerical study of laminar methane-air triple flames in two-dimensional mixing layers. They reported that the interaction between the diffusion and premixed flame branches present in a triple flame significantly affected the local burning velocity in certain regions in a triple flame. They concluded that radiation had negligible effect on local burning properties in a triple flame. Wada et al. (2009) experimentally and numerically studied flame interactions of partially premixed flames in terms of variation of strain rate in counter flowing methane-air streams under atmospheric conditions. They reported that the flame width decreases as strain rate increases for the same level of premixing, and at extinction the flame width values remains almost constant.

The brief literature review presented above indicates that a number of work have been performed in the field of counter flowing partially premixed methane-air flames. The effect of the combination of the equivalence ratios of rich and lean streams and the strain rate involved, on the structure of the partially premixed flame, especially its transition from a triple flame to a double flame and subsequently to a single flame structure, is of academic interest. In this paper, such a systematic analysis is carried out using a simplified and yet a comprehensive validated numerical model with detailed C2 chemistry. Further, the rates of important reactions those form the major kernels of the flame structure are also investigated.

2 Numerical model

A combustion model is setup using the commercial CFD software, FLUENT 6.3 (2005) by choosing appropriate model parameters such as second order upwind scheme for convection terms and SIMPLE algorithm for velocity-pressure coupling, and by using a user defined function for incorporating optically thin radiation model (Barlow et al., 1999). The present numerical model closely follows the features of a validated reacting flow model reported in Sreenivasan et al. (2011). The general governing equations for mass, momentum, species and energy conservation in the gas-phase are given below in vector form.

(1) *Continuity equation*

$$\frac{\partial \rho}{\partial t} + \nabla.(\rho \vec{V}) = 0 \tag{1}$$

(2) *Momentum equation*

$$\frac{\partial (\rho \vec{V})}{\partial t} + \nabla.(\rho \vec{V}\vec{V}) = -\nabla p + \nabla.\vec{\tau} + \rho \vec{g}, \tag{2}$$

where p is the static pressure, $\vec{\tau}$ is the stress tensor, $\rho\vec{g}$ is the gravitational body force and $\vec{V}$ is the velocity vector. The stress tensor $\vec{\tau}$ is given by

$$\vec{\tau} = \mu\left[(\nabla \vec{V} + \nabla \vec{V}^T) - \frac{2}{3}\nabla.\vec{V}I\right],$$

where μ is the molecular viscosity, I is the unit tensor, and the second term on the right hand side is the effect of volume dilation.

(3) *Species conservation equations*

Fluent predicts the value of the local mass fraction of each species, Y_i, through the solution of a scalar transport equation for each species. This conservation equation takes the following general form:

$$\frac{\partial}{\partial t}(\rho Y_i)+\nabla.(\rho\vec{V}Y_i)=-\nabla.\vec{J}_i+R_i+S_i, \quad (3)$$

where $\vec{J}_i$ is the diffusive flux of species i, which arise due to concentration gradients, R_i is the net mass rate of production of species i by chemical reaction and S_i is the appropriate source term. An equation of this form will be solved for *N-1* species, where N is the total number of gas-phase chemical species used in the system. Since the mass fraction of the species must sum to unity, the mass fraction of the N^{th} species is determined as one minus the sum of the *N-1* solved mass fractions. To minimize numerical error, the N^{th} species is selected in the present numerical model as the species with overall largest mass fraction, that is, nitrogen (N_2). A full multi-component species transport model is used as the reacting flow is dominated by diffusion as well as convection. Multi-component diffusion in a laminar flow is calculated using the species diffusive mass flux vector, $\vec{J}_i$ and the Maxwell-Stefan equation as given below.

$$\vec{J}_i=-\sum_{j=1}^{N-1}\rho D_{ij}\nabla Y_j,$$

where Y_j is the mass fraction of species j, D_{ij} is the binary mass diffusion coefficient defined as follows:

$$D_{ij}=[D]=[A]^{-1}[B],$$

$$A_{ii}=-\left(\frac{X_i}{D_{iN}}\frac{M_w}{M_{w,N}}+\sum_{j=1,j\neq i}^{N}\frac{X_j}{D_{ij}}\frac{M_w}{M_{w,i}}\right),$$

$$A_{ij}=X_i\left(\frac{1}{D_{ij}}\frac{M_w}{M_{w,j}}-\frac{1}{D_{iN}}\frac{M_w}{M_{w,N}}\right),$$

$$B_{ii}=-\left(X_i\frac{M_w}{M_{w,N}}+(1-X_i)\frac{M_w}{M_{w,i}}\right),$$

$$B_{ii}=X_i\left(\frac{M_w}{M_{w,j}}-\frac{M_w}{M_{w,N}}\right),$$

where $[A]$ and $[B]$ are $(N-1)\times(N-1)$ matrices, M_w is the molecular weight and X_i is the mole fraction of species i.

(4) *Energy equation*

The energy conservation equation, which includes enthalpy transport by species and radiative heat flux losses, is given by,

$$\frac{\partial}{\partial t}(\rho C_pT)+\nabla.(\rho\vec{V}C_pT)=\nabla.(k\nabla T)-\sum_{i=1}^{N}R_i\Delta h_{f,i}+\sum_{i-1}^{N}[\nabla.(\rho D_{ij}C_{p,i}T\nabla Y_i)]+q''_R, \quad (4)$$

where, $\Delta h_{f,i}$ is the enthalpy of formation for i^{th} species, q''_R is the radiation heat flux absorbed by the species. The governing equations have been solved until steady state is reached in a segregated manner with double precision accuracy. A laminar species transport model with volumetric reactions is used along with finite rate chemistry. Full multi-component diffusion along with a diffusion energy source is used to model the species diffusion. Arrhenius rate equation is used to obtain the rate of formation or destruction of all the species. The net rates of formation of several species participating in the multiple chemical reactions have been solved simultaneously using a stiff chemistry solver. The chemical kinetics mechanism employed in this study is based on GRI 2.11, in which all C3 and higher order species, and nitrogen containing species, except N_2, have been removed. This mechanism consists of 121 reactions with 25 species. Thermophysical properties of the species have been calculated as functions of temperature and species concentrations (Reid et al., 1981, McBride et al., 1993).

The axisymmetric computational domain is shown in Fig. 1. It consists of two ducts kept co-axially opposing each other, separated by a distance L. A fuel rich mixture of methane and air flows from the bottom duct and a fuel lean mixture flows out from the top as shown in Fig. 1. The diameters of the duct are taken as 25 mm. The velocities of the counter flowing streams, the equivalence ratios and the separation distance, L, can be varied to obtain a desired strain rate following Seiser et al. (2007). After a thorough study, an extended domain is employed in the simulations having an additional radius of 60% of the duct radius.

The domain has been divided in to several quadrilateral control volumes. Structured grids are used with uniform spacing in the radial and axial directions. After carrying out thorough grid independence study, the cell sizes in axial and radial directions are fixed as 0.025 mm. The boundary conditions used are listed below.

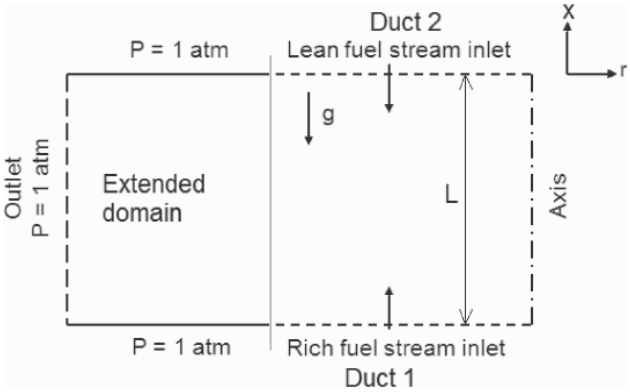

Fig. 1: Schematic of the computational domain along with the boundary types

Duct inlets: At this boundary, average axial velocities (V_1 and V_2, subscripts 1 and 2, represent bottom and top ducts, respectively), temperatures and mass fractions of methane, oxygen and nitrogen are specified. Fully developed velocity profile is prescribed.

Pressure specified boundaries: The boundaries on the top as well as on the bottom of the extended domain (Fig. 1) are specified as pressure inlet conditions, available in FLUENT. When air entrains into the domain, an oxygen mass fraction of 0.232 and a constant ambient temperature of 300 K are specified at these boundaries.

Outlet: At the exit boundary, flow leaves to the atmosphere. Therefore, a pressure outlet condition, which drives the flow with respect to local pressure gradient, has been chosen at this boundary. In case of backflow into the domain oxygen mass fraction of 0.232 and a constant temperature of 300 K are specified.

Axis: This boundary represents the centerline of the burner. For the axisymmetric problem, an axis boundary condition, available in FLUENT, has been specified (Fig. 1); the boundary conditions are: radial velocity, $U_r = 0$ and $\partial\phi/\partial r = 0$, where ϕ is any other variable.

The velocity, temperature and species mass fractions are initialized to some constant values across the computational domain. Appropriate under relaxation factors are set for updating pressure, density, body force, momentum, species and temperature. Cold flow simulation is executed for around 2500 to 3000 iterations till a reasonable convergence is obtained. Then, at a few cells near the axis, in the mid-way between the ducts, a high temperature (≈ 1500 K) is set to onset ignition. The case is executed for around 5000 iterations, after which the occurrence of ignition is checked and the optically thin radiation model is turned on. The case is executed till convergence is obtained. The convergence criterion for all the equations is that the difference between the current and the previous iteration value is below 1×10^{-6}.

3 Validation of the numerical model

To validate the numerical model, the present numerical predictions are compared against the experimental measurements reported Ravikrishna and Laurendeau (2000). Methane-air stream with an equivalence ratio of 1.45 is injected into the domain at $x = 0$ m and an opposed stream of air alone is injected at an axial distance of $x = 0.02$ m. In Fig. 2, the axial temperature profile obtained by present numerical model is compared with the measured values and that predicted by the numerical model reported in Ravikrishna and Laurendeau (2000). There is a reasonably good agreement between the results from the present numerical model and the experimental data (Ravikrishna and Laurendeau, 2000). The measured temperatures are 100–200 K higher than the predictions, at the locations between $x = 0.006$ m to 0.0125 m, which produces a maximum error of around 10%. Hence, it can be concluded that the current numerical model is able to predict the structure of opposed flames quite well.

To further validate the numerical model for a case where premixed methane-air streams exit from both the ducts, the experimental measurements reported in Smooke et al. (1988) has been used. A case, where $V_1 = 0.82$ m/s, $V_2 = 0.597$ m/s, $T_1 = 299.15$ K, $T_2 = 303.15$ K, mass fractions of fuel in bottom ($x = 0$) and top ($x = L = 0.015$ m)

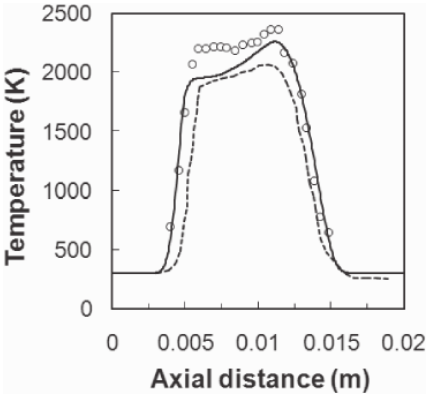

Fig. 2: Temperature profile along the axis predicted by the present model (solid line) compared with the experimental (symbols) and numerical data (dashed line) of Ravikrishna and Laurendeau (2000)

ducts equal to 0.526 and 0.027, and those of oxygen equal to 0.108 and 0.223, respectively, has been considered. This gives equivalence ratio values of bottom and top streams as 18.8 and 0.48, respectively. Numerically predicted profiles of temperature, axial velocity and concentrations of species along the axis have been compared with the corresponding experimentally measured values (Smooke et al., 1988).

The present numerical results and the results of Smooke et al. (1988) for axial velocity show satisfactory agreement at almost every point in the flow field starting from the rich stream side up to a location before the occurrence of a local minimum (Fig. 3). Near the lean mixture stream side, the axial velocity predictions deviate significantly as compared to the experimental values. The occurrence of the local minimum in the axial velocity is due to the expansion of hot gases in the flame zone. It can be noted that the numerical results presented in Smooke et al. (1988) is able to predict the velocity profile at the leaner stream side quite well, however, at the richer stream side, there are notable discrepancies.

Figure 3(b) shows the predicted temperature profile along the axis, along with the numerical and experimental results of Smooke et al. (1988). It is seen that the maximum temperature and its location are predicted quite satisfactorily. As opposed to the velocity profile prediction (Fig. 3a), the temperature profile near the lean stream side is predicted quite accurately by the present numerical model (Fig. 3b) as compared to the rich stream side. It can be noted that the comparison of present numerical model is similar to that reported in Smooke et al. (1988). Profiles of several species predicted by the numerical model are compared with those reported in Smooke et al. (1988). The predicted concentration of CH_4, as shown in Fig. 3(c), rapidly approaches zero at two positions, indicating the presence of two reaction zones. This is further explained in Fig. 4. This trend matches well with the measured values.

Overall the comparison of the present numerical results against those predicted by Smooke et al. (1988) is quite good. The location of the fuel consumption, for both the fuel rich premixed zone and the fuel lean premixed zone is predicted very well. The predicted concentrations of O_2 and N_2 are nonzero, as observed in experiments (Fig. 3c). Since the concentration of oxygen is nonzero everywhere, it can be concluded that enough amount of oxygen is available for the formation of the rich premixed flame located near the exit of rich stream ($x = 0$ m) and

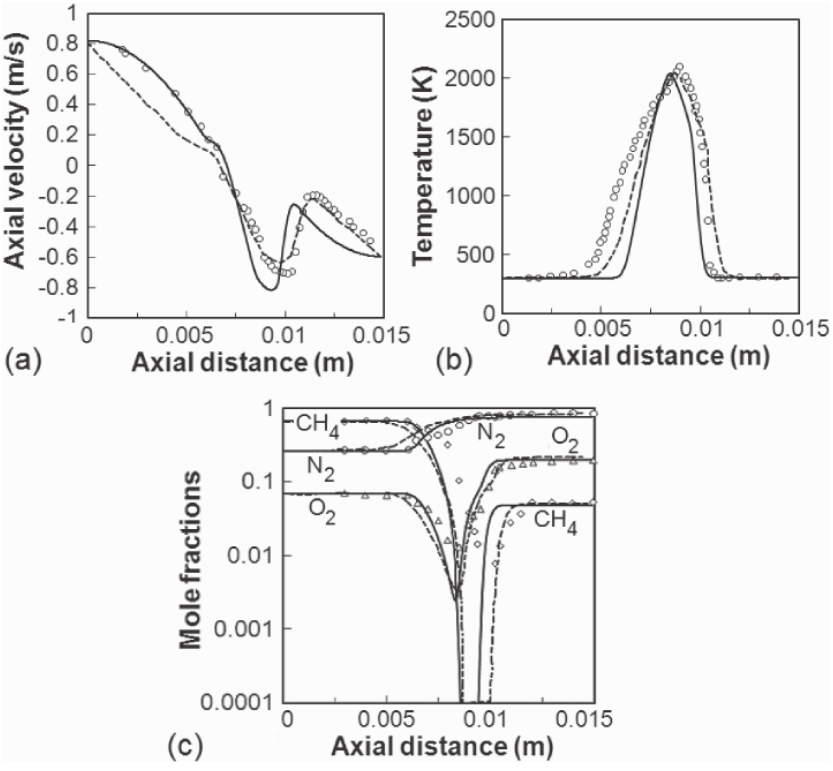

Fig. 3: (a) Axial velocity profile (b) Temperature profile and (c) profiles of CH_4, N_2, O_2 along the axis predicted by the present model (solid lines) compared with the experimental data {symbols: CH_4 (◊), N_2 (○), O_2 (Δ)} and the numerical values (dashed line) of Smooke et al. (1988)

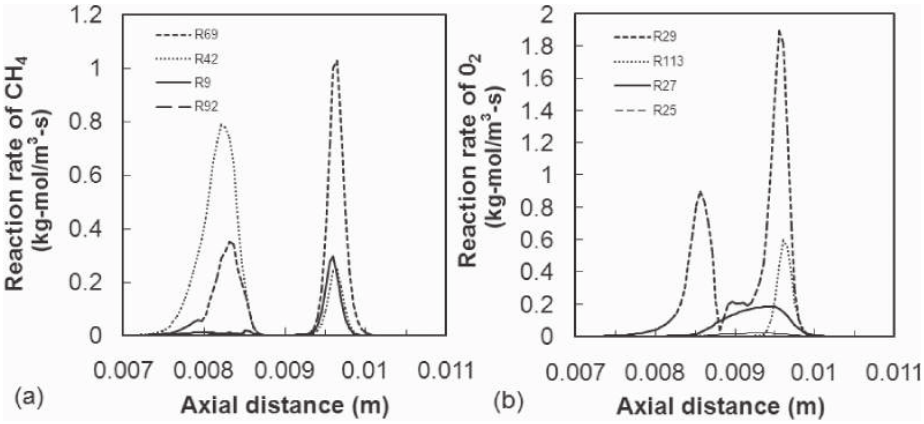

Fig. 4: (a) Methane and (b) Oxygen consumption by important elementary reactions

lean premixed flame located near the exit of lean stream ($x = 0.015$ m), and both flames have kinetic interactions.

4 Results and discussion

First of all, investigation of the overall rates of important reactions those consume methane and oxygen is carried out for the validation problem discussed in Fig. 3. This would explain the two flame zones present in that problem. By investigating all the reactions involving methane, four reaction steps are identified to consume methane substantially, as given below.

$$\text{R69: } OH + CH_4 \Leftrightarrow CH_3 + H_2O$$

$$\text{R42: } H + CH_4 \Leftrightarrow CH_3 + H_2$$

$$\text{R9: } O + CH_4 \Leftrightarrow OH + CH_3$$

$$\text{R92: } CH + CH_4 \Leftrightarrow H + C_2H_4$$

Figure 4(a) shows the CH_4 consumption rates profiles as given by the selected reactions. Two peaks are observed indicating two locations at which methane is consumed – one located near the rich premixed stream ($x \approx 0.008$ m), and other near the lean premixed stream ($x = 0.009$ m). Each of them is formed by two different reaction steps given by reactions R69 and R42 at the lean- and rich-premixed sides, respectively. This shows that methane is consumed predominantly by OH on the lean premixed zone and by H on the rich premixed zone. These peaks are completely separated because of low strain rate in this case. It is also observed that O and CH radicals also play important roles in CH_4 consumption. However they are overshadowed by the reactions involving OH and H radicals.

Oxygen consumption takes place through 18 elementary reactions. The important reactions those predominantly consume oxygen can be arranged in the descending order of their overall reaction rates as follows:

$$\text{R29: } H + O_2 \Leftrightarrow O + OH$$

$$\text{R113: } HCO + O_2 \Leftrightarrow HO_2 + CO$$

$$\text{R27: } H + O_2 + H_2O \Leftrightarrow HO_2 + H_2O$$

$$\text{R25: } H + O_2 + M \Leftrightarrow HO_2 + M$$

Figure 4(b) show the oxygen consumption by the reactions listed above. Similar to the methane reaction profiles, the oxygen consumption occurs in two locations.

However, only one single reaction, defined by R29, forms the major reaction that consumes oxygen. This chain branching reaction produces two radicals, O and OH, by the reaction between H and O_2. On the lean side reaction R113 becomes the second notable reaction. The production of HO_2 and CO by this reaction forms one of the major kernels for the flame on the lean premixed side. The other two reactions involving oxygen and hydrogen atom, R27 and R25, are reactions involving a third body; in R27, the third body is H_2O. These reactions are hence slower; especially the last recombination reaction is observed to be the slowest. Reaction rates are higher at the lean premixed zone due to the availability of excess oxygen.

The structure of the flame formed in counter-flowing partially premixed streams is subject to changes as the strain rate is varied. At a critical value of this strain rate, the flame gets extinguished. The strain rate (a) is defined following the method reported by Seiser et al. (2007) as follows:

$$a = \frac{2|V_2|}{L}\left(1 + \frac{|V_1|}{|V_2|}\sqrt{\frac{\rho_1}{\rho_2}}\right) \tag{5}$$

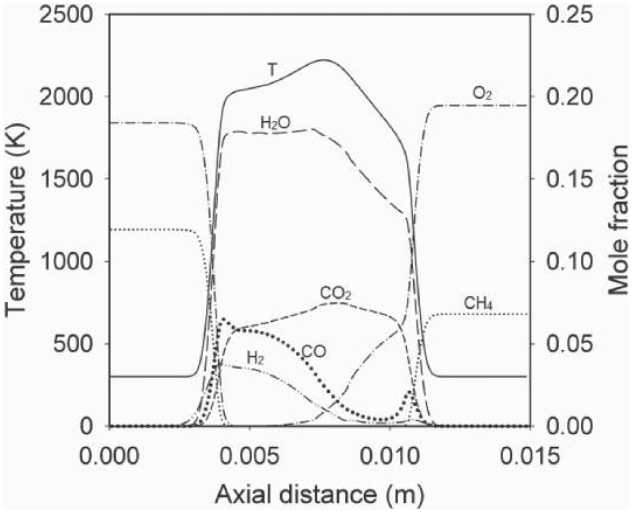

Fig. 5: Numerically predicted temperature and species profiles for a flame with $\phi_{lean} = 0.7$, $\phi_{rich} = 1.3$ and a strain rate of 135 (1/s), showing a triple flame structure

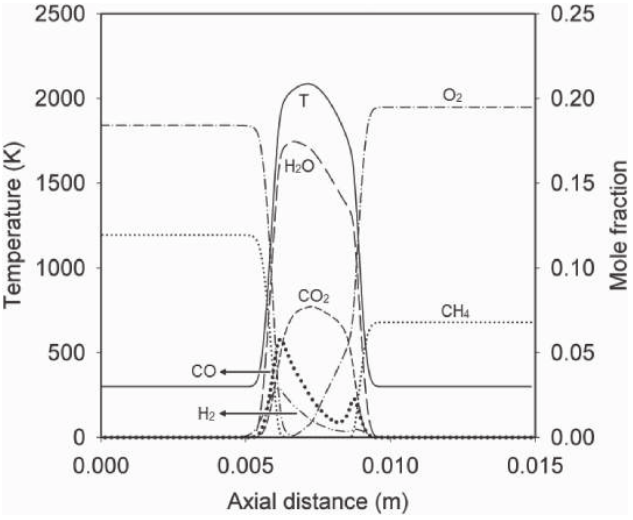

Fig. 6: Numerically predicted temperature and species profiles for a flame with $\phi_{lean} = 0.7$, $\phi_{rich} = 1.3$ and a strain rate of 405 (1/s), showing a double flame structure

In equation (5), ρ represents the density of the reactant mixture at the exit of the corresponding ducts. Further, the momentum of each stream in counter-flowing reactant streams ($\rho_i V_i^2$, $i = 1, 2$) is kept the same so that the stagnation plane is formed approximately at the mid-distance between the ducts. The variation in the structure is also dependent on the equivalence ratios (ϕ) of the approaching streams. To understand the effect of all these parameters, a case with the lean side equivalence ratio of 0.7, the rich side equivalence ratio of 1.3 and a strain rate of 135 (1/s), is simulated. The flame structure for this case is shown in Fig. 5, which represents a triple flame. The flame consists of a lean premixed flame located near the lean side ($x = 0.015$ m), a rich premixed flame located near the rich side ($x = 0$) and a diffusion flame formed in between them, which has the maximum temperature. It can be noted that the temperature from the left side increases and plateaus through a small distance after its sharp increase and then increases again. Similarly there is a distinct, significant change in slope of the temperature profile from the right side towards the peak. This indicates the presence of three flame zones. Sharp increase in CO_2 near the lean and rich stream sides, and its local maximum at a location near to the stagnation plane, shows the triple flame configuration. Local CO peaks on rich and lean sides forms the consumption locations for methane. The peak value of CO in the rich side is more than that of CO_2. In the middle flame, CO consumption adds to CO_2 addition, and its variation is non-linear.

For getting a double flame, keeping the same rich and lean equivalence ratio values as in the previous case, the strain rate is increased to 405 (1/s). The flame structure is shown in Fig. 6. The overall reaction zone thickness has reduced (Wada et al., 2009). The existence of two reaction zones, one near the rich side and another near the lean fuel side can be noticed. The peak temperature has also decreased. The temperature profile in this case is much smoother than the previous case as two flame zones exist with a small overlap in this case. Methane is consumed in two layers and its concentration from both the left and right streams approaches almost zero value at locations where CO reaches its peak, indicating that it is fully consumed at these two reaction zones. The variation of CO within the flame zone is significantly different for this case as compared to the triple flame case and its rich peak value is less than that of CO_2. Also CO_2 variation does not have a local maximum near stagnation plane as in the previous case.

For getting a single flame structure, the strain rate is further increased to 1620 (1/s). The flame structure obtained is shown in Fig. 7, in which an almost thin reaction zone is observed due to increased stretch (Wada et al., 2009). The variation of the temperature profile, closeness of the methane consumption zones and smooth CO_2 profile indicates that only single flame zone exists. The peak temperature has also decreased, which can be attributed to the aerodynamic heat loss with increase in strain rate, known as strain-induced cooling.

With another pair of equivalence ratios equal to 0.25 and 1.25, the temperature profiles along the axis have been plotted for various strain rates ranging from 200 (1/s) to 1600 (1/s) in Fig. 8. The double flame structure at a

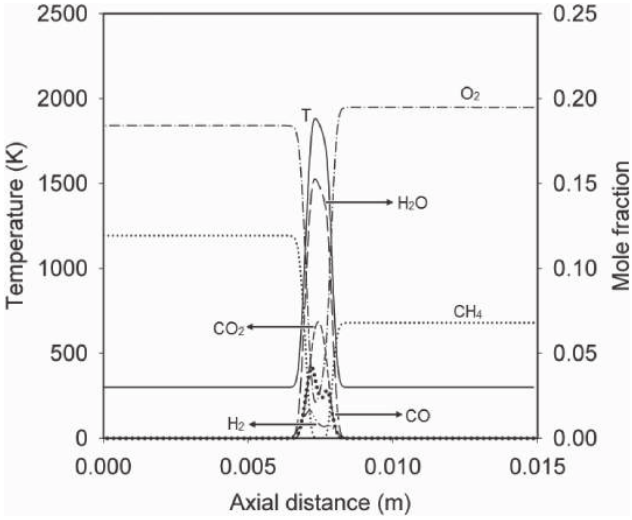

Fig. 7: Numerically predicted temperature and species profiles for a flame with $\phi_{lean} = 0.7$, $\phi_{rich} = 1.3$ and a strain rate of 1620 (1/s), showing a single flame structure

strain rate of 200 (1/s) changes to single flame structure at 600 (1/s) as shown in Fig. 8. This is consistent with the observations for the previous case and the reasons for the same are discussed above. Significant reduction in the maximum temperature value occurs as the strain rate is increased. As mentioned earlier, this can be attributed to the aerodynamic heat loss due to increase in the strain rate, called strain-induced cooling. When the strain rate is increased to 1000 (1/s), the peak temperature slightly decreases.

When the strain rate is further increased to 1400 (1/s), the temperature profile shows a steep increase around an axial location of $x = 0.006$ m. However, it can be noted that the peak temperature has increased for this case. Also at this strain rate, the thin flame zone has shifted towards the rich side. The very thin flame zone is formed as a result of increased strain rate. For this higher strain rate case, the convective strengths of both the streams are sufficient to influence the flame zone thickness. As the flame zone thickness reduces, the heat release within a smaller volume has caused increased temperature for this case.

When the strain rate is further increased, at its value of around 1600 (1/s), flame extinguishes. Therefore, it is clear that prior to extinction, the flame exhibits a thin single reaction zone (Wada et al., 2009). The critical value of strain rate at which extinction occurs depends strongly on the equivalence ratio of the opposing streams. For a given set of equivalence ratios, a unique strain rate is required to cause flame extinction.

5 Summary

The structure and extinction characteristics of laminar flames formed between counter-flowing methane-air streams having rich and lean equivalence ratios have been predicted using a numerical model. The numerical model uses a chemical kinetics sub-model involving a mechanism of 121 elementary reaction steps and 25 species and an optically thin radiation sub-model. Thorough validation of the numerical model has been carried out using double flame structure data of Smooke et al. (1988) as well as that of Ravikrishna and Laurendeau (2000). At low strain rates, three reaction zones, corresponding to lean premixed zone, rich premixed zone and a diffusion zone in between these are observed, representing a triple flame. In the triple flame zone, the temperature from the left side increases and plateaus through a small distance after its sharp increase and then increases again. Similarly there is a distinct, significant change in slope of the temperature profile from the right side towards the peak. With increase in strain rate, the triple flame transits to a double flame,

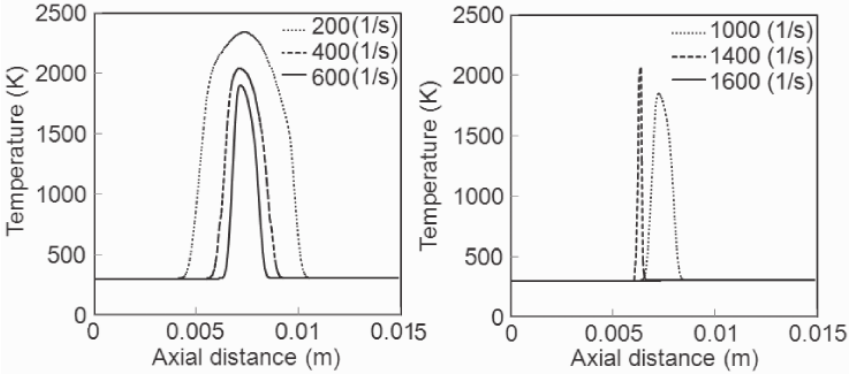

Fig. 8: Numerically predicted temperature profiles along the axis for cases with $\phi_{lean} = 0.25$ and $\phi_{rich} = 1.25$, for various strain rates

which has a rich premixed and a lean premixed reactions zone in it. With further increase in the strain rate, a single reaction zone results. The variation of the temperature profile, closeness of the methane consumption zones and smooth CO_2 profile indicates that only single flame zone exists. Further increase in the strain rate causes flame extinction. The separation distance between the reaction zones decreases as strain rate increases for the same level of premixing. The maximum temperature in the domain also show a decreasing trend with strain rate because of the strain induced cooling. Before extinction, a very thin flame zone is formed as a result of increased strain rate where the convective strengths of both the streams are sufficient to influence the flame zone thickness. As the flame zone thickness reduces, the heat release within a smaller volume has caused increased temperature for this case.

Received: August 01, 2012. Accepted: August 01, 2012.

References

Barlow, R. S., Smith, N. S. A., Chen, J. Y., Bilger, R. W. Nitric oxide formation in dilute hydrogen jet flames: isolation of the effects of radiation and turbulence-chemistry submodels. Combust. Flame. 1999; 117:4–31.

Blevins, L. G. and Gore, J. P. (1998) Computed structure of low strain rate partially premixed CH_4-air counter-flow flames: Implications for NO Formation, *Combustion and Flame*, 116, 546–556.

Fluent User Guide. Fluent 6.3.26, 2005 and http://www.fluent.com.

Guo, H., Liu, F. and Smallwood, G. J. (2006) A numerical study of laminar methane/air triple flames in two-dimensional mixing layers, *International Journal of Thermal Sciences*, 45, 586–594.

Hamins, A., Thridandum, H. and Seshadri, K. (1985) Structure and extinction of counter-flow partially premixed diffusion flame, *Chemical Engineering Science*, 40, 2027–4038.

McBride, B. J., Sanford, G. and Reno, M. A. Coefficients for calculating thermodynamic and transport properties of individual species. NASA Tech. Memorandum 4513, 1993.

Nishioka, M., Nakagawa, S., Ishikawa, Y. and Takeno, T. (1994) NO Emission characteristics of methane-air double flame, *Combustion and flame,* 98, 127–138.

Ravikrishna, R. V. and Laurendeau, M. N. (2000) Laser-induced fluorescence measurements and modeling of nitric oxide in counter-flow partially premixed flames, *The Combustion Institute*, 122, 474–482.

Reid, R. C., Prausnitz, J. M., Sherwood, T. K. The properties of gases and liquids. Third Edition. McGraw-Hill Book Company. New York. 1981.

Rogg, B., Behrendt, F. and Warnatz, J. (1986) Turbulent non-premixed combustion in partially premixed diffusion flamelets with detailed chemistry, *21st Symposium (International) on Combustion/The Combustion Institute*, 1533–1541.

Seiser, R., Humer, S., Seshadri, K. and Pucher, E. (2007) Experimental investigation of methanol and ethanol flames in nonuniform flows, *Proceedings of the Combustion Institute 31*, 1173–1180.

Seshadri, K., Puri, I. and Peters, N. (1985) Experimental and theoretical investigation of partially premixed diffusion flames at extinction, *Combustion and Flame,* 61, 237–249.

Smooke, M. D., Seshadri, K. and Puri, I. K. (1988) The structure and extinction of partially premixed methane burning methane in air, *22nd Symposium (International) on Combustion/The Combustion Institute*, 1555–1563.

Sreenivasan, R., Raghavan, V. and Sundararajan, T., (2011) An investigation of flame zones and burning velocities of laminar unconfined methane-oxygen premixed flames, Combustion theory and modeling, DOI:10.1080/13647830.2011.606918.

Tanoff, M. A., Smooke, M. D., Osborn, R. J., Brown, T. M. and Pitz, R. W. (1996) The sensitive structure of partially premixed methane-air vs. air counter-flow flames, *26th Symposium (International) on Combustion/The Combustion Institute*, 1121–1128.

Wada, T., Mizomoto, M., Yokomori, T. and Peters, N. (2009) Extinction of methane-air counter-flow partially premixed flames, *Proceedings of the Combustion Institute*, 32, 1075–1082.

Xue, H. S., Aggarwal, S. K., Osborn, R. J., Brown, T. M. and Pitz, R. W. (2002) Assessment of reaction mechanisms for counter-flow methane-air partially premixed flames, *AIAA Journal*, 40, 1236–1238.

Yamaoka, I., Tsuji, H. and Harigaya, Y. (1986) Extinction and structure of methane/very lean methane air counter flow diffusion flames, *21st Symposium (International) on Combustion/The Combustion Institute*, 1837–1843.